Volume 2
Number 7
7 April 2021
Pages 2143–2446

Materials Advances

rsc.li/materials-advances

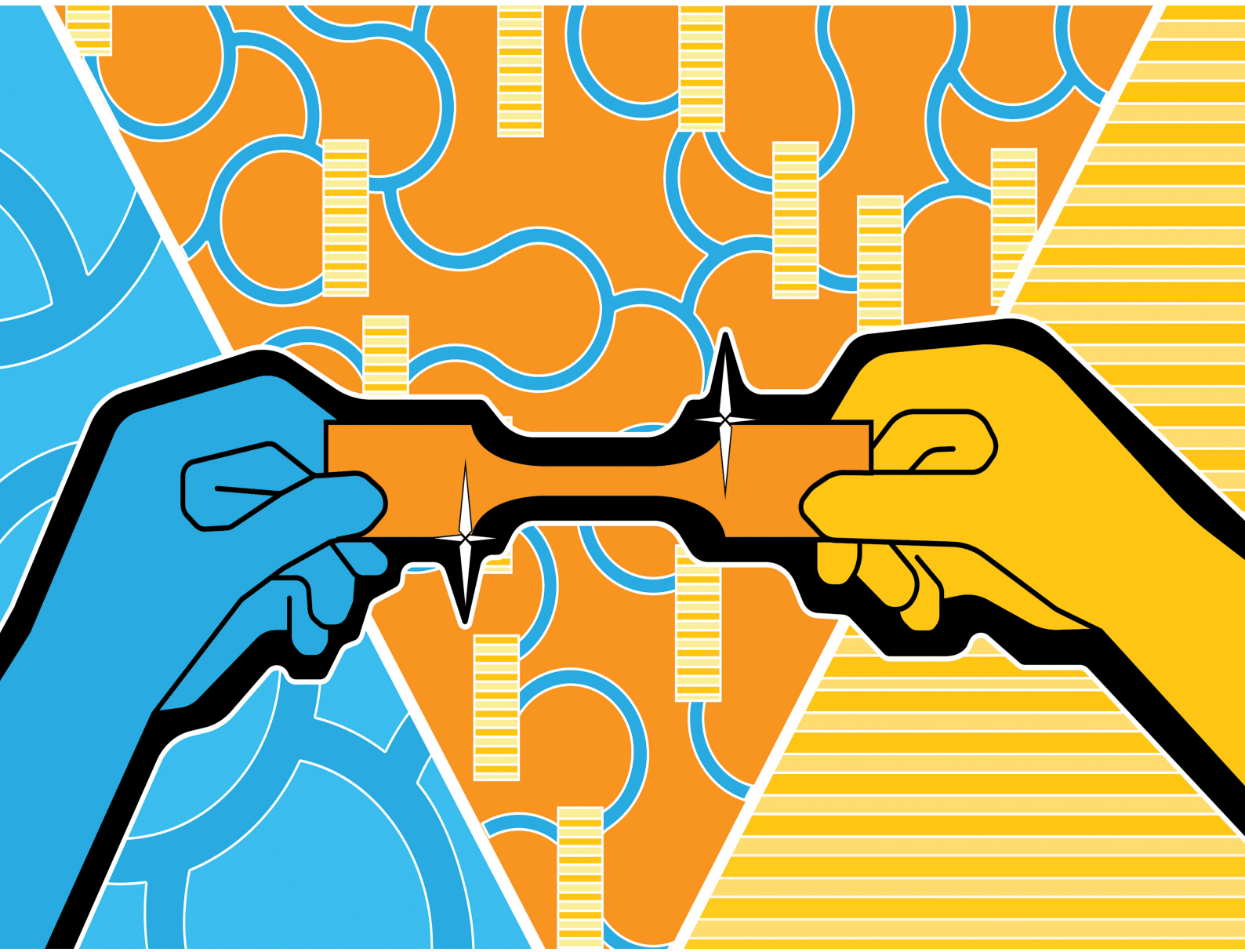

ISSN 2633-5409

ROYAL SOCIETY OF CHEMISTRY

PAPER
Thomas Konegger, Miriam M. Unterlass *et al.*
High modulus polyimide particle-reinforcement of epoxy composites

Materials Advances

ROYAL SOCIETY OF CHEMISTRY

PAPER

View Article Online
View Journal | View Issue

Cite this: *Mater. Adv.*, 2021, **2**, 2278

High modulus polyimide particle-reinforcement of epoxy composites†

Johannes Essmeister, [a] M. Josef Taublaender, [bc] Thomas Koch,[d] D. Alonso Cerrón-Infantes, [bce] Miriam M. Unterlass [bce] and Thomas Konegger *[a]

In this work, a novel class of fully organic, lightweight composite materials was prepared by incorporating highly crystalline, hydrothermally synthesized poly(*p*-phenylene pyromellitimide) (PPPI) microparticles into a commercial epoxy matrix. Particle loadings of up to 15 vol% could be achieved. Microstructural, mechanical, and thermal properties of these composites were investigated by scanning electron microscopy, three-point bending and Vickers hardness testing, dynamic mechanical analysis, nanoindentation, and thermogravimetric analysis. The incorporation of the PPPI filler particles into the epoxy matrix was found to be homogeneous. Powder X-ray diffraction shows that PPPI's crystallinity is retained in the composites, and infrared spectroscopy indicates a covalent bonding of PPPI to the epoxy matrix. Flexural modulus and storage modulus were increased by the PPPI addition, while the flexural strain at break was reduced. In contrast to that, the flexural strength remained unaffected by the incorporation of PPPI filler particles. Raising the filler content also resulted in an improvement of hardness. Furthermore, a decrease in glass-transition temperature with increasing PPPI content was observed, as well as a pronounced increase in thermal stability of the composites in comparison to the unfilled cured epoxy resin. These results indicate the high potential of this new class of composites with prospective applicability *e.g.* in the fields of sports equipment, aerospace, and automotive technology.

Received 14th December 2020,
Accepted 29th January 2021

DOI: 10.1039/d0ma00980f

rsc.li/materials-advances

1. Introduction

Polyimides (PIs) are a popular class of organic high-performance polymers (HPPs) that exhibit remarkable properties including high specific strength, high modulus, and high temperature stability.[1] These advantageous materials properties are known to be even enhanced further with increasing crystallinity.[2] Therefore, efforts to synthesize highly ordered PIs have been made in the past.[3,4] However, generally one of the downsides of generating PIs is that the conventional synthetic routes require toxic solvents, harmful condensation catalysts, as well as long reaction times at elevated temperatures (typically at least 300 °C). In stark contrast to that, hydrothermal polymerization (HTP) is a much greener alternative for synthesizing PIs by using nothing but water under high-pressure and high-temperature conditions.[5,6] On top of allowing for generating PIs in solely water, HTP furthermore generates them at high order. Recent work has shown that PIs bearing some degree of flexibility in their backbone are obtained as fully crystalline product by HTP, but as fully amorphous product when synthesized classically.[7,8] The rigid-chain polyimide poly(*p*-phenylene pyromellitimide) (PPPI) is hydrothermally also generated at unprecedentedly high crystallinity, while classically synthesized PPPI features nematic order at best.[5] Furthermore, HTP provides an opportunity to obtain microparticles with a plethora of different morphologies, tunable through employing additives during HTP.[6] However, the rigidity of PPPI's polymer backbone – clearly beneficial from the viewpoint of materials properties – also leads to the absence of any softening phenomena (melting or glass transition) upon heating, as well as PPPI's practically complete insolubility in virtually any common solvent. HTP generates fully condensed PPPI, *i.e.* PPPI of such a high degree of polymerization that end-groups cannot be detected at high crystallinity, which renders solubility and softening phenomena even less conceivable. Fully crystalline PPPI is generally hardly processable,[3,5] since conventional techniques from solution or melt are inherently

[a] *TU Wien, Institute of Chemical Technologies and Analytics, Getreidemarkt 9/164-CT, 1060 Vienna, Austria. E-mail: thomas.konegger@tuwien.ac.at*
[b] *TU Wien, Institute of Materials Chemistry, Getreidemarkt 9/165, 1060 Vienna, Austria*
[c] *TU Wien, Institute of Applied Synthetic Chemistry, Getreidemarkt 9/163, 1060 Vienna, Austria*
[d] *TU Wien, Institute of Materials Science and Technology, Getreidemarkt 9, 1060 Vienna, Austria*
[e] *CeMM – Research Center for Molecular Medicine of the Austrian Academy of Sciences, Lazarettgasse 14, AKH BT 25.3, 1090 Vienna, Austria*

† Electronic supplementary information (ESI) available. See DOI: 10.1039/d0ma00980f

not employable. However, one possibility to circumvent these processing issues, whilst taking advantage of the enhanced crystallinity of hydrothermally generated PPPI, is to incorporate the obtained microparticles into a processable matrix material for yielding novel types of composites.

Generally, the fabrication of composites by incorporation of various types of fillers into a multitude of different polymer matrices is a broad field of research. Among all matrix materials, epoxy systems hold a unique position due to their industrial importance, their broad availability, and the adjustability of various of their materials properties through the choice of molecular backbone. Most commonly, epoxy matrices are reinforced by incorporating inorganic particles such as ZrO_2, SiO_2, Al_2O_3, diamond, glass, short carbon fibres, and nano-clays,[9–17] which results in an enhancement of mechanical and/or thermal properties. These inorganic filler particles typically increase the modulus and fracture toughness of the composites. However, the strengthening effect strongly depends on the interfacial adhesion and size of the particles.[18] In addition to inorganic particles, the incorporation of organic-based fillers, which inherently provide a better interface (due to comparably high chemical similarity between the two phases), has also turned out to be suitable for improving the properties of epoxy-based systems. Among others, various types of rubbers, thermoplastics, or organically-modified graphene have been shown to be potent filler materials.[19–21] However, for certain filler materials one has to deal with some drawbacks, and a trade-off between certain properties has to be found. In case of the use of rubber particles for example, a toughening effect can be achieved, with the drawback of reducing modulus and, in most cases, strength.[22] Contrary to that, for thermoplastic-modified epoxy systems an even higher toughening effect can be achieved without experiencing a severe decrease in Young's modulus and tensile strength.[22,23] Examples for thermoplastics introduced into an epoxy matrix include polyphenyleneoxide, poly(methyl methacrylate), or polycarbonate.[20] Moreover, as shown by Cho *et al.*, polyetherimide has successfully been applied to strengthen and toughen epoxy systems without simultaneously reducing the flexural modulus.[24] For doing so, the polyetherimide was incorporated into the epoxy resin using a solution-based process forming separate inclusions during curing.[25] In addition to that, other works such as a recent publication by Chen *et al.* on PI-fiber-reinforced epoxy composites also suggest that PI fillers can help to simultaneously improve both modulus and strength.[26] These reports clearly indicate the suitability and compatibility of PIs as high-performance fillers for epoxy matrix systems.

Since hydrothermally generated PPPI particles themselves inherently exhibit exceptional intrinsic properties (stemming from their high degree of crystallinity) including remarkable thermal and potentially high mechanical characteristics, we were intrigued to investigate their potential as filler material for epoxy matrix-based composites. Thus, with this study we were not only aiming towards developing a strategy for preparing novel types of fully organic composite materials consisting of hydrothermally synthesized PPPI filler particles and a commercially available epoxy matrix, but also aimed at evaluating the effect of PPPI addition on the resulting materials properties. Consequently, the obtained composite materials were intensively characterized regarding their mechanical properties such as strength and hardness, as well as their thermal behaviour including glass-transition temperature and thermal degradation. Based on these investigations, we will discuss the advantages and limits of these novel types of composite materials, thus providing a framework for prospective application scenarios in fields such as sports equipment, aerospace, and automotive applications.

2. Experimental section

2.1 Preparation of PPPI filler particles

PPPI was synthesised as previously reported by Taublaender *et al.* within the framework of a two-step reaction.[6] After the initial formation of a suitable monomer salt precursor, HTP was carried out to yield the desired highly crystalline PPPI microparticles. An outline of the main synthetic steps is given in the following two paragraphs.

To synthesize the monomer salt, 42.4 g (194.4 mmol, 1.08 eq.) of pyromellitic dianhydride (PMDA, 98%; Sigma-Aldrich) were added to 600 mL of degassed distilled H_2O. After stirring at 80 °C under Ar atmosphere for one hour, the solution cleared, indicating completion of the hydrolysis to pyromellitic acid (PMA). 19.5 g (180 mmol, 1 eq.) of *p*-phenylenediamine (PDA, 97%; Sigma-Aldrich) were added, leading to the precipitation of the monomer salt as an off-white solid. The monomer salt was separated by vacuum filtration, washed intensely with distilled H_2O, and dried under vacuum conditions at room temperature.[6]

Subsequently, 23.9 g of the dry monomer salt (66 mmol) were suspended in 330 mL of distilled water in a 1000 mL steel autoclave in order to perform the HTP towards PPPI. After properly closing the autoclave, the mixture was heated to 250 °C for 3 h under stirring. The reaction was stopped by rapidly quenching the autoclave with cold tap H_2O to room temperature. The obtained orange product was separated by vacuum filtration and washed with distilled water and ethanol. Finally, the isolated PPPI powder was dried at 80 °C under vacuum overnight.[6] No further milling or deagglomeration treatments were conducted before subsequent processing.

2.2 Preparation of epoxy composites

As matrix polymer, a commercial epoxy system consisting of a DGEBA prepolymer (diglycidylether of bisphenol-A) and an amine-hardener formulation (2,4-diethyl-6-methyl-1,3-phenylenediamine; 1,2-diaminocyclohexane) was used (Huntsman; Araldite LY 1564/Hardener XB 3473). For the preparation of the composites, the dried PPPI microparticles were initially suspended in isopropanol. For varying the PPPI volume content in the final composites (which was varied between 5 vol% and 20 vol%), the quantity of PPPI introduced into isopropanol was

adjusted in accordance to the amount of epoxy mixture subsequently used, typically ranging from 2 g to 7 g of PPPI per 150 mL isopropanol. In order to break up particle agglomerates, the PPPI/isopropanol mixture was treated in an ultrasonic bath (Bandelin, Sonorex Super AK 106) for 60 minutes and under a probe sonicator (Hielscher, UP400S) for 15 minutes (70% amplitude, 0.5 cycle). The respective quantity of epoxy prepolymer (DGEBA) was mixed with the obtained isopropanol/PPPI slurry using a dispersing instrument (Ultra Turrax, T25 basic) for 60 minutes at 1900 rpm. Subsequently, isopropanol was removed from the mixture by rotary evaporation at 60 °C. After the addition of the curing agent, the highly viscous prepolymer/PPPI mixture was homogenized using a planetary mixer (Thinky, ARE-250; 4 minutes at 2000 rpm). Subsequently, the mixture was degassed in the planetary mixer for 10 minutes at 800 rpm and then for 20 minutes at 20 mbar. Before the desired PPPI-filled epoxy specimens were cast, the rectangular silicone moulds (Wacker, Elastosil M 4641 B, mould dimensions 100 × 35 × 10 mm) were coated with a thin layer of silicone spray (Wacker, Silicone spray AK). Additionally, it was found to be beneficial if both composite mixture and silicone moulds were preheated to 90 °C before the composite mixture was finally cast into the moulds. The subsequent curing routine included an initial step at 130 °C for 3 hours followed by 12 hours at 160 °C. Unfilled epoxy reference samples (PPPI content 0%) were prepared by mixing the epoxy prepolymer (DGEBA) with the amine-hardener formulation in a weight ratio of 100 to 26 parts, respectively. The mixture was stirred in a planetary mixer for 4 minutes at 2000 rpm. Degassing and casting were carried out using the same procedure as for the composite samples. The scheme of preparation of the composite samples is presented in Fig. 1.

2.3 Characterization

Mechanical characterization was performed *via* three-point bending tests using a Zwick 1474 universal testing machine following the EN ISO 178 protocol. The cast and cured samples were cut into test specimens and ground and polished to the testing dimensions (35 × 5 × 1.60 mm). The tensile surface was polished to a 1 μm finish using diamond media. For each PPPI content, 10 samples were tested using a support span of 25.4 mm and a test speed of 1 mm min^{-1}. Vickers hardness testing was performed using a load of 9.81 N (HV1) on polished sample cross-sections (EMCO test M4U-025 hardness tester). Nanoindentation was performed using a loading of 0.5 mN, a loading rate of 0.05 mN s^{-1}, 30 s holding time, and 0.1 mN s^{-1} release on polished sample cross-sections. Details on the determination of the indentation modulus of PPPI particles are included in the ESI.† Dynamic mechanical analysis (DMA) was performed in a three-point bending setup with a support span length of 20 mm (test specimens dimensions of 35 × 5 × 1.25 mm) at 1 Hz and 0.06% dynamic strain (TA Instruments, DMA Q800), and the temperature was varied from 30 °C to 250 °C at a heating rate of 3 K min^{-1}. Thermogravimetric analysis (TGA) was conducted using a PerkinElmer TGA 8000 instrument with a ramp of 10 K min^{-1} from 30 °C to 700 °C under flowing nitrogen atmosphere (20 mL min^{-1}). For TGA analyses, the samples were cryo-milled with a vibration mill and liquid nitrogen cooling (Retsch, Mixer Mill MM 400). The crushed samples were then sieved and the fraction between 200 μm and 90 μm was used for analysis. Powder X-ray diffraction was performed with a PANAlytical X'Pert Pro at a diffraction angle 2θ between 5° and 60° using a CuK_α source. The same powdered samples were used for TGA measurements. Scanning electron microscopy (SEM) images of fracture surfaces and polished samples were recorded using a FEI ESEM Quanta 200. SEM images of PPPI particles were recorded after preparation by sprinkling the dry PPPI powder on carbon-tape coated steel sample holders and subsequent sputtering with an 8 nm thick layer of Au/Pd 60/40 alloy with a Quarum Q105T S sample preparation system. Imaging was carried out with a Quanta 200F FEI microscope. The samples were measured at 5 kV, with a working distance of 9 mm and spot size 2.0. Note that the PPPI powders were obtained after HTP by (i) filtration, (ii) washing with distilled water, and (iii) drying in a vacuum oven at 80 °C. After this isolation procedure PPPI is obtained as storable, dry powder.

Attenuated total reflectance infrared spectroscopy (ATR-FT-IR) was conducted on a Bruker Tensor 27 working in ATR MicroFocusing MVP-QL with a diamond crystal, using OPUS (version 4.0) software for data analysis. Resolution was set to 2–4 cm^{-1}, and spectra were recorded from 4000 to 470 cm^{-1}.

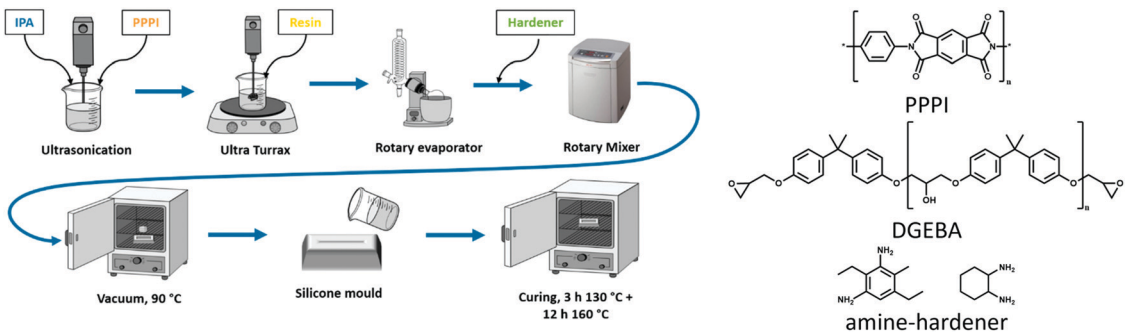

Fig. 1 Scheme for the preparation of epoxy-based composites and chemical structures of (*p*-phenylene pyromellitimide) (PPPI), epoxy prepolymer (DGEBA), and amine-hardener.

3. Results and discussion

3.1 Characterization of PPPI filler particles

Before discussing the PPPI/epoxy composites regarding their preparation and properties, characteristics of the used filler particles should be briefly elucidated here. Further details can be found in the corresponding literature (*cf.* ref. 6). As can be seen from the SEM image taken from a representative PPPI powder sample depicted in Fig. 2, the PPPI particles used in this work almost exclusively exhibit a sheet-like structure. The particle size (*i.e.* the length, width, and thickness of the particles) was determined from SEM images, and was found to be in the range of ~0.5–5 μm (length), 0.5–3 μm (width), and ~0.2 μm (thickness), see representative SEM image in Fig. 2. From SEM images it becomes clear that while the majority of the particles is found to be at the upper end of the determined size range (approximately 4–5 μm × 2–3 μm × 0.2 μm), there is also a second population at the lower end of the size range (approximately 0.5 μm × 0.5–1 μm × 0.2 μm). Furthermore, many particles are crystalline aggregates of intergrown platelets, which is prompted through their synthesis by hydrothermal polymerization,[5,6] and hence expected. The observed particle morphology in Fig. 2 results exclusively from the hydrothermal polymerisation and was not altered by further grinding or deagglomeration processes.

The sheet-like structure of the PPPI particles implies a high aspect ratio (length/thickness), which is promising for yielding enhanced reinforcement due to a higher surface area and more efficient stress transfer from the matrix to the filler. On the one hand, this sheet-like geometry can be expected to be beneficial for the use in polymer-based composites.[27,28] On the other hand, it is also conceivable that the full crystallinity of the PPPI platelets imparts brittleness, *i.e.* allows for the platelets to fracture in parallel to the PPPI chain orientation in the crystalline platelets.

3.2 Composite fabrication and initial characterization

For the preparation of the desired composite materials it was clearly of the utmost importance to ensure proper dispersion of PPPI in the liquid matrix precursor DGEBA, as well as successful degassing in order to avoid structural inhomogeneities and void formation, respectively. Preheating of the used moulds as well as of the still liquid prepolymer/PPPI slurry prior to the casting process furthermore turned out to be highly advantageous for yielding high-quality specimens. Moreover, it already became evident during the first composite fabrication experiments that a filler content higher than 15 vol% could not be achieved due to a steep increase in viscosity upon elevating the amount of PPPI introduced.

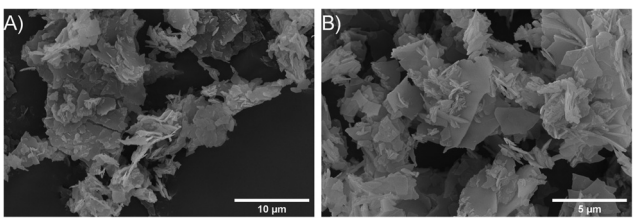

Fig. 2 SEM micrographs showing the sheet-like morphology of hydrothermally generated PPPI products at different magnifications.

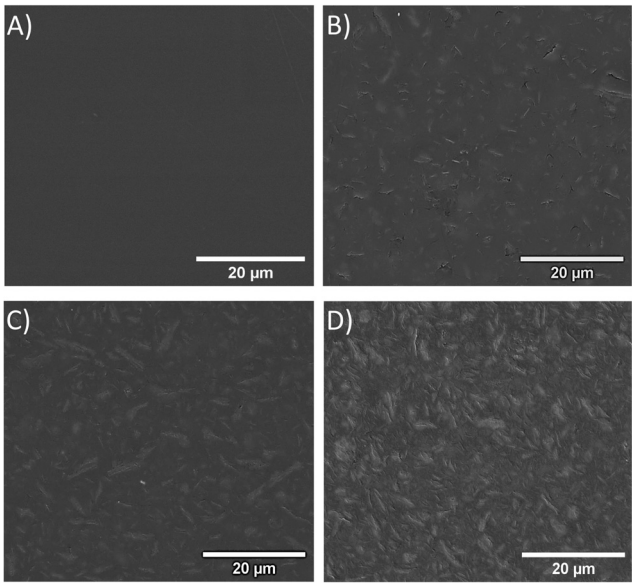

Fig. 3 Backscatter-SEM micrographs of polished (A) neat epoxy and PPPI-reinforced epoxy composites containing (B) 5 vol% (C) 10 vol% (D) 15 vol% PPPI.

For assessing the internal composite structure and filler particle distribution, scanning-electron microscopy (SEM) images of the polished sample surfaces were taken in backscattered electron (BSE) mode. Here, PPPI particles are visible as brighter spots embedded in the surrounding darker epoxy matrix. As Fig. 3 indicates, the PPPI microsheets are homogeneously distributed in a random orientation. Furthermore, the size and geometry of the embedded PPPI particles is nicely comparable with the starting particles. Hence, the PPPI particles did not fracture significantly into smaller pieces during composite preparation. Furthermore, breaking-out of the PPPI particles during polishing can be observed. This is probably due to the rigid nature of PPPI and the resulting brittleness of the microparticles. In fact, this issue could not be avoided even when attempting various rather careful and gentle cutting or polishing techniques such as ultramicrotomy. Consequently, these difficulties in sample preparation, *i.e.* the breaking-out of filler particles, can already be expected to render nanoindentation measurements of PPPI particles rather challenging. Furthermore, this phenomenon may also negatively affect mechanical behaviour during the three-point bending tests of polished PPPI-reinforced epoxy composites.

Furthermore, we performed powder X-ray diffraction (PXRD) of the powdered composites as well as of pristine PPPI and the unfilled epoxy matrix. PPPI displays high crystallinity as evinced through the presence of all major and minor reflections (Fig. 4A, top diffraction curve), as previously reported.[5] In contrast, the unfilled epoxy matrix features only one amorphous halo centered around 17° (2θ, Cu-K_α), *cf.*

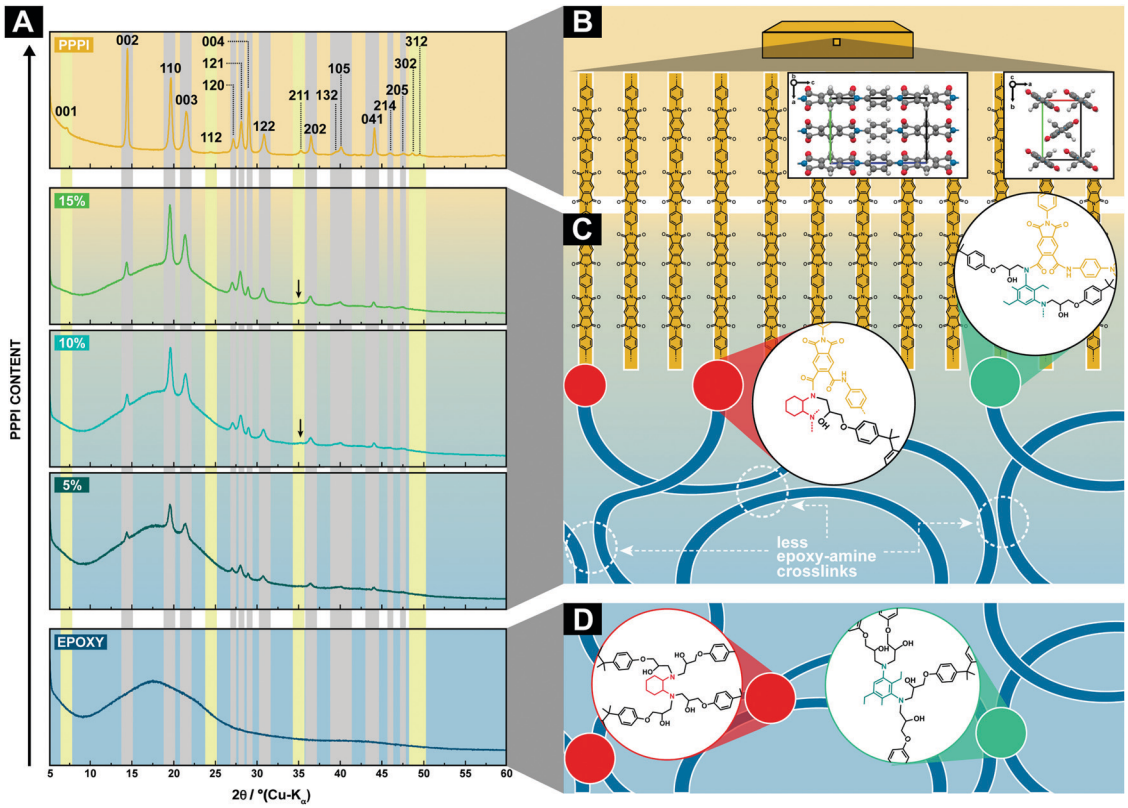

Fig. 4 PXRD analysis of the used PPPI filler (A, top curve), the pristine epoxy matrix (A, bottom curve), and the composites of PPPI filler contents of 5 vol% (A, second curve from bottom), 10 vol% (A, third curve from bottom), and 15 vol% (A, second curve from top). (*hkl*) of all PPPI reflections are indicated; gray background highlights reflections that are retained in the composites, and yellow background indicates reflections that are not or only partly (arrows) retained. (B) Schematic of the structure of PPPI platelets; (C) schematic of the composites' structure indicating the proposed covalent linking of PPPI to the epoxy matrix *via* amides with the used amine hardeners; (D) schematic of the unfilled epoxy system's structure.

Fig. 4A, bottom curve. In the composites, the majority of PPPI's reflections are retained and sit on top the amorphous halo contributed by the epoxy. The retained reflections are highlighted by gray background in Fig. 4A, and these are: (002), (110), (003), (120), (121), (004), (122), (202), (132), (105), (041), (214), and (205). There are four reflections of PPPI that are not retained in any of the three composites, *i.e.* (001), (112), (302), and (312), and one reflection that can only be seen in samples with 10 and 15 vol% PPPI, namely (211), indicated by arrows. These not/partly retained reflections are highlighted in Fig. 4A with light yellow background, and are already very weak in pristine PPPI. Therefrom, we can overall conclude that the PPPI particles (i) remain sufficiently intact through composite processing to retain their crystallinity, and, as expected, (ii) the intensity of the reflections and visibility of even very weak reflections scales with the amount of PPPI in the composite. Fig. 4B furthermore illustrates the structure of PPPI platelets schematically and shows PPPI's crystal structure. A schematic of the unfilled (Fig. 4D) and filled (Fig. 4C) epoxy resin includes the partial covalent bonding of the PPPI filler to the epoxy matrix, which we infer from ATR-FT-IR analysis, as discussed subsequently.

Attenuated total reflectance Fourier transform infrared (ATR-FT-IR) spectroscopy was furthermore performed on the powdered composite samples, as well as on the powdered pristine PPPI and reference epoxy resin, and is shown in Fig. 5. The spectra of all three composites contain both the modes of the epoxy matrix and of PPPI, and their intensity scales nicely with the relative amount of PPPI:epoxy. For instance, the OH-mode of the epoxy resin at $\sim$3400 cm^{-1} decreases in intensity with increasing PPPI content (*cf.* Fig. 5B), and the strongest mode of PPPI at $\sim$1710 cm^{-1} increases in intensity with the composites' PPPI content (Fig. 5C). In addition, the appearance of two weak features points at an amide linkage between PPPI and the amine hardener (a mixture of 2,4-diethyl-6-methyl-1,3-phenylenediamine and 1,2-diaminocyclohexane; *i.e.* Huntsman; Araldite LY 1564/Hardener XB 3473). Specifically, we find a weak shoulder at 2700 cm^{-1}, which is neither present in PPPI nor in the unfilled cured epoxy. We suspect that this mode corresponds to an amide A mode, which is typically found in the region of 3500–3000 cm^{-1}, but can be found at 2700 cm^{-1} when H-bonding to the amide carbonyl is present.[29] Moreover, the most indicative mode for imides is in PPPI found as a *ca.* 10 cm^{-1} broad peak with its maximum at 1710 cm^{-1}, while in all composites, this broad peak's maximum is shifted to 1725 cm^{-1}, which falls into the region of amide 1 modes (Fig. 5C). Clearly, these two features are weak in intensity and an indication rather than a proof of amide bonding. We hypothesize that such amide linkages exist

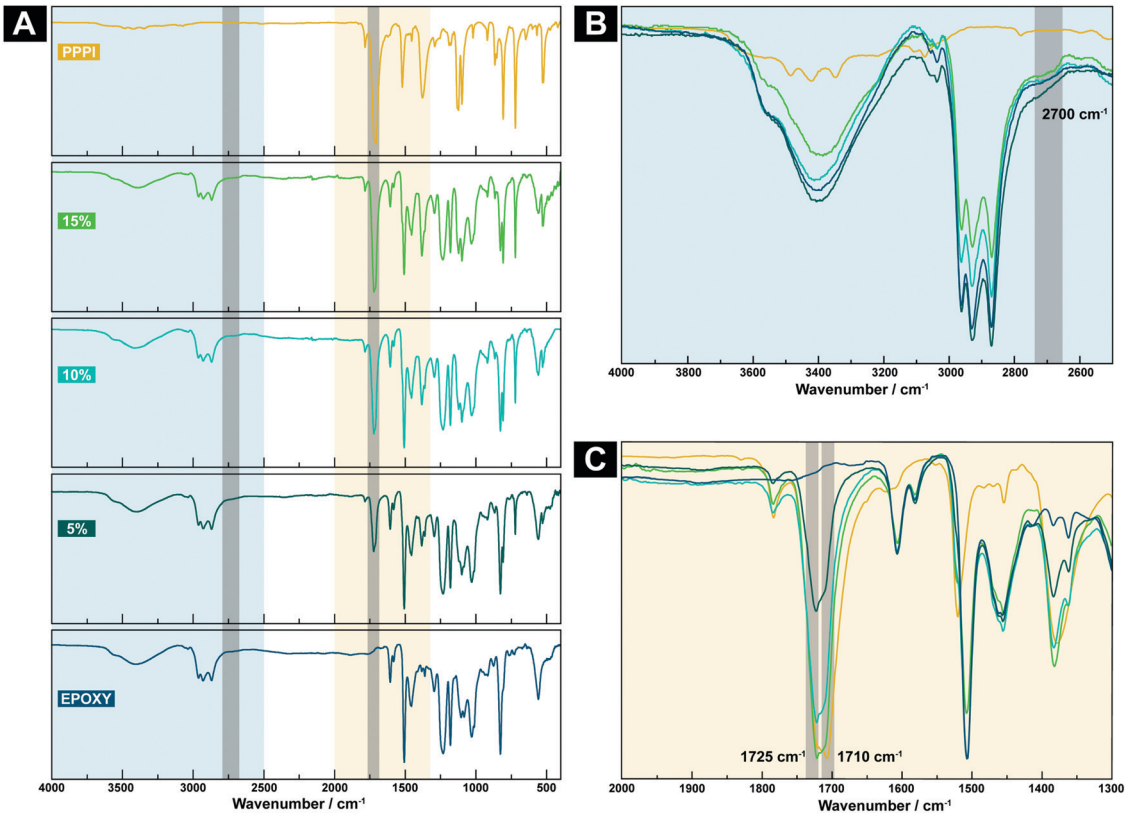

Fig. 5 ATR-FT-IR spectra of the composite and pristine PPPI and unfilled epoxy. (A) Individual spectra of all five materials from 4000–470 cm^{-1}. (B) Overlay of the spectra in the region of 4000–2500 cm^{-1}. (C) Overlay of the spectra in the region of 2000–1300 cm^{-1}. Gray boxes highlighting modes at ~2700 cm^{-1} and 1725 cm^{-1} are indicative for amides.

in the composites, as illustrated schematically in Fig. 4C, yet that the ratio of amide functions to all other functions is relatively small, hence their low intensity in ATR-FT-IR.

3.3 Mechanical properties

3.3.1 Three-point bending tests. To investigate the mechanical behaviour in the elastic and plastic range of the material until failure, three-point bending tests were carried out. In Fig. 6, representative stress/strain curves of the prepared composite specimens as well as of an unfilled epoxy reference sample are shown. Table 1 lists the averaged flexural properties determined therefrom. Clearly, the addition and the amount of PPPI cause a significant change of the mechanical properties. From Fig. 6 and Table 1 it readily becomes evident that with increasing PPPI content the generated composite materials show a decrease in flexural strain at break and an increase in flexural modulus, whereas the flexural strength is almost unaffected by the filler content. The plasticity of the composite decreases progressively with the amount of PPPI until an almost complete lack of plastic behaviour is observed for the composite containing 15 vol% PPPI.

The flexural strength of the composite material does not change significantly compared to the unfilled epoxy, no increase in flexural strength was observed with increasing PPPI content. This result is however not fully unexpected for composites reinforced with particles in the lower micron size range. In the literature, such decreases in flexural strength have indeed been reported for polymer composites reinforced with micron-sized rigid particles.[18]

After mechanically characterizing the prepared composites, SEM fractograms (see Fig. 7 for representative images taken

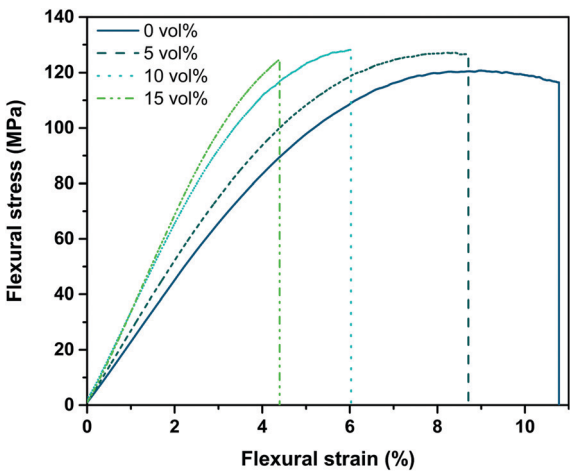

Fig. 6 Representative stress/strain curves obtained from three-point bending tests of PPPI-reinforced epoxy-composites for specimens containing different amounts of PPPI filler.

Table 1 Flexural modulus E_f, flexural strength σ_{fM}, and flexural strain at break ε_{fB} of PPPI-reinforced epoxy-composites as a function of PPPI content

PPPI (vol%)	E_f (MPa)	σ_{fM} (MPa)	ε_{fB} (%)
0	2200 ± 98	120 ± 2	10.0 ± 0.8
5	2480 ± 77	124 ± 2	9.3 ± 1.0
10	2910 ± 110	126 ± 3	6.0 ± 0.6
15	3200 ± 95	123 ± 4	4.5 ± 0.4

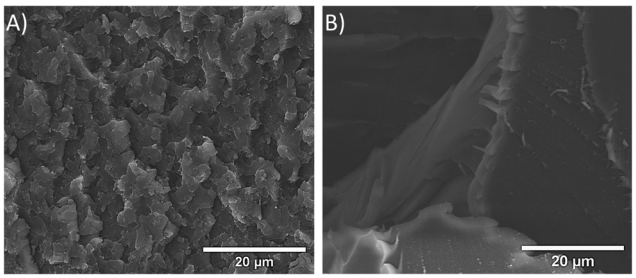

Fig. 7 SEM micrographs showing the fracture surfaces of PPPI-reinforced epoxy composites: (A) epoxy reinforced with 10 vol% PPPI; (B) neat epoxy.

from composites containing 10 wt% PPPI) were recorded in order to give a better understanding of the failure mechanisms present. In the unfilled epoxy reference specimen, brittle fracture is indicated by the smooth, glass-like surface. In contrast, the composite materials exhibit a step-like fracture surface, indicating debonding of filler particles oriented parallel to the direction of fracture from the surrounding matrix. This phase separation of parallelly oriented particles in further consequence results in crater formation on the fracture surface, the size of which corresponds to the particle size. Additionally, no debonding of particles oriented perpendicularly to the fracture surface can be observed, which would be indicated by sharp, small cavities originating from a pull-out of these particles. Therefore, particles oriented perpendicularly to the fracture surface most likely break.

Based on these two failure mechanisms of differently oriented particles, adequate to strong interface adhesion between filler particles and matrix can be assumed. Potentially, this good adhesion between the two phases stems from a reaction occurring between the amine hardener and surface imide moieties of PPPI particles. Similarly, so-called aminolysis reactions are generally well-known to occur on the surface of PI materials (*e.g.* films) in the presence of various types of primary amines,[30] and the hardener used in the epoxy curing here is in fact an amine. Furthermore, for nanocomposites with bad wetting (i.e., a subpar interface) between the polymeric matrix and the nanoparticulate fillers, it has been shown that that the filler often resides inside voids and is not in direct contact with the matrix. In contrast, favourable interfacial interaction is microscopically characterized by direct contact between matrix and filler.[31] As both SEM fractograms (Fig. 7) and BSE micrographs of the polished samples (Fig. 3) show good contact between matrix and filler and no voids, we believe that the interaction between both is rather favourable in the case of the here prepared composites, or at least not unfavourable. Yet, more detailed analysis would be necessary to properly assess the interfaces, which is considered for future studies.

As opposed to the flexural strength, the flexural modulus shows an almost linear increase with PPPI content. To estimate the theoretical boundaries of modulus enhancement, empirical models were applied. The rule of mixture (ROM) and the inverse rule of mixture (inverse ROM) given in eqn (1) and (2), respectively, are two straightforward approaches for doing so. Both models require the knowledge of the flexural modulus and volume fraction of the matrix, E_m and V_m, as well as the modulus and volume fraction of the filler compound, E_f and V_f.[32,33] While E_m is easily available from bulk measurements from non-reinforced reference samples, the determination of E_f is significantly more challenging. In the present case, utilizing the indentation modulus of 8700 ± 1060 MPa (obtained from nanoindentation measurements on PPPI particles embedded in a polyimide matrix, see ESI† for further details) was found to provide a suitable estimation for E_f. In further consequence, the obtained E_f and E_m values allow for a satisfactory prediction of the behaviour of the composite modulus.

$$E_c = E_f V_f + E_m V_m \quad (1)$$

$$E_c = \left(\frac{V_f}{E_f} + \frac{V_m}{E_m}\right)^{-1} \quad (2)$$

The Halpin–Tsai model is one of the most used models to estimate the modulus of composite materials, as estimations on filler geometry and orientation can be applied. This approach (see eqn (3) and (4)) uses the moduli of both components (*i.e.* E_f and E_m) as well as a factor ζ – which takes the filler geometry into account – to estimate the modulus of the composite E_c. In a rough approximation, the filler geometry can be assumed to be ellipsoidal and randomly oriented, leading to a factor of $\zeta = 3$. The constant η, which contains the ratios between the filler and matrix moduli as well as the geometry factor ζ, is usually written separately to simplify the illustration.[10,18,34]

$$\frac{E_c}{E_M} = \frac{1 + \zeta\eta V_f}{1 - \eta V_f} \quad (3)$$

$$\eta = \frac{\left(\frac{E_f}{E_m}\right) - 1}{\left(\frac{E_f}{E_m}\right) + \zeta} \quad (4)$$

The Kerner equation (eqn (5)) allows for predicting E_c. For doing so, the Poisson's ratio ν_m (taken from literature as 0.35 [9]), the modulus of the matrix material E_m, and the volume fraction of the filler compound V_f are required.[10,18,33] This equation predicts the modulus of the composite only by assuming spherical particles and takes no other geometrical assumptions into account, hence assuming a perfect interfacial adhesion and an isotropic, homogeneous composite.

$$\frac{E_c}{E_m} = 1 + \frac{15V_f(1 - \nu_m)}{(1 - V_f)(8 - 10\nu_m)} \quad (5)$$

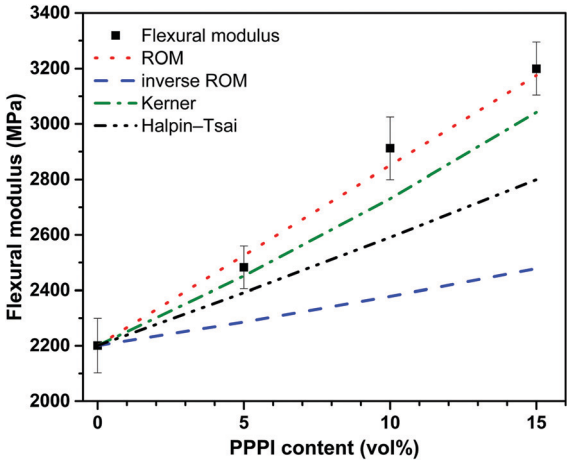

Fig. 8 Flexural modulus of PPPI-reinforced epoxy composites as a function of PPPI content comparing the measured values with the relationship predicted by four different estimation models.

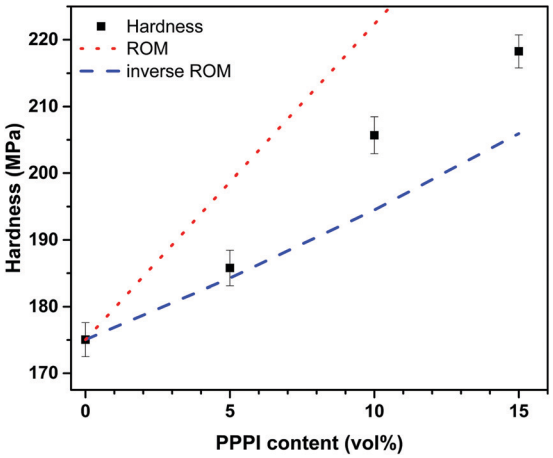

Fig. 9 Hardness (HV1) of PPPI-reinforced epoxy composites as a function of PPPI content comparing the measured values with the relationship predicted by ROM and inverse ROM, respectively.

In Fig. 8, the measured flexural moduli as well as the ones predicted by the four estimation models presented are plotted for different PPPI contents. Generally, the ROM approach indicates the upper bound for a property of a given composite material, while the inverse ROM method marks the lower bound.[35,36] In the present case, the behaviour predicted by ROM is in good accordance with the measured flexural composites modulus, indicating that the indentation modulus determined for the PPPI particles by nanoindentation is plausible.

As can be clearly seen in Fig. 8, the Halpin–Tsai and Kerner equations underestimate the flexural modulus of the composites. The significant deviation observed is most likely caused by the approximations required for these equations, including particulate geometry and orientation.

3.3.2 Hardness. The Vickers hardness (HV1) of the composite materials increases nearly linearly with PPPI filler content. For all composites up to filler contents of 15 vol%, no cracks were formed at the indentation edges, thus ruling out a highly brittle material behaviour. In accordance to the above described procedures for predicting the flexural moduli of our composites, we also tried to estimate the hardening effect of PPPI *via* ROM and inverse ROM. The hardness of the pure PPPI particles was determined to be 648 ± 83 MPa by nanoindentation and used in eqn (1) and (2) as H_f (replacing E_f). The hardness of the epoxy matrix, determined *via* Vickers hardness testing (175 ± 3 MPa), was used in eqn (1) and (2) as H_m (replacing E_m). As clearly becomes evident in Fig. 9, the actually measured composite Vickers hardness lies between the respective curves predicted by ROM and inverse ROM. Hardness is typically overestimated when using smaller indenters (as was the case for the nanoindentation setup), which may affect the measured hardness of the PPPI particles, and may explain the deviation between the measured composite data and the behaviour predicted both by ROM and inverse ROM.

3.4 Thermomechanical properties

The viscoelastic behaviour of the materials as a function of temperature was evaluated by DMA (Fig. 10). As to be expected from the previous results, the storage modulus at room temperature increases upon elevating the PPPI content – comparable to the behaviour of the flexural modulus determined from three-point bending tests. In terms of temperature dependency, a strong effect of the particle content on the thermomechanical properties was observed. With rising PPPI content, the transition between the glass-like and rubbery regions (indicated by the tangent delta of the phase angle between storage and loss modulus) is shifted to lower temperatures. A particularly pronounced decrease in storage modulus occurs for the sample containing 15 vol% PPPI. This can be described best by observing the peak of tan delta (Fig. 10), which can be assigned to the glass transition temperature (T_g) of the material. Clearly, a significant decrease in T_g is observed upon increasing the filler content. T_g decreases from 174 °C in the unfilled epoxy to 159 °C at 5 vol% PPPI, and to 156 °C at 10 vol% PPPI. An even stronger decrease in T_g to 117 °C can be observed in the sample

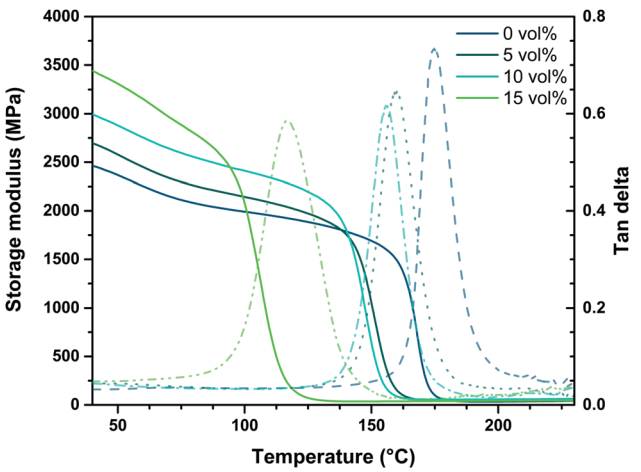

Fig. 10 Storage modulus and tan delta *versus* temperature of PPPI-reinforced epoxy composites for specimens containing different amounts of PPPI filler.

containing 15 vol% PPPI. This observation was at first glance surprising to us, as we expected PPPI – for its thermal features (reported decomposition temperature T_D is ~640 °C), absence of T_g or melting point,[5] and outstanding calculated stiffness and strength (theoretical calculation on the PPPI chain have predicted a modulus of 500 GPa)[2] – to impart an increase in T_g compared to the unfilled epoxy. The literature reports increases in T_g with increasing filler content for micron-sized fillers,[37–39] but also decreases in T_g for instance for nanocomposites.[40,41] In general, it appears that the effect of the filler and its content on T_g strongly depends on the interface between filler and matrix. In our composites, we believe to have good interfacial interaction between epoxy and PPPI due to their direct contact and absence of voids deduced from SEM images, and for their – to some degree – covalent linking *via* amide bonds. However, the covalent linkage between PPPI and epoxy consumes some of the hardener molecules, and therefore must decrease the crosslinking density in the epoxy matrix (*cf.* illustration in Fig. 4C). We attribute the decrease in the composites' T_g with the PPPI content to this decrease in matrix crosslinking density.

Furthermore, it should be noted that the reduction of peak height in Fig. 10 implies a decreased dampening of the material with rising PPPI content. This result can be expected due to the rigidity of PPPI, and implies a good interface between filler and matrix, since mobility of the molecular chains at the interface decreases. Furthermore, a broadening of the peaks is noticeable, which can be related to heterogeneity in the composites.[9,15,42] This peak broadening is particularly pronounced in the composite containing 15 vol% PPPI, indicating a comparably high degree of heterogeneity in this sample.

In Fig. 11, the storage modulus at 30 °C is plotted against the PPPI content. As previously applied for the flexural modulus, the same four prediction models were applied to accordingly evaluate the trend in storage modulus. Again, the indentation modulus of PPPI was used as the filler modulus E_f, and the storage modulus of the epoxy reference sample (2510 MPa) was used as the matrix modulus E_m. In the filler concentration range observed, both ROM and the Kerner equation predict the relationship between storage modulus and PPPI content very accurately. In this case, the Kerner equation displays a steep progression, as it tends to overestimate the composite modulus when a higher matrix modulus is applied for modelling.[33] As the measured storage modulus of the neat epoxy has a higher value than the measured flexural modulus (2200 MPa), the Kerner equation shifts more closely to the ROM in this filler concentration range. In case of the Halpin–Tsai model, the modulus is again underestimated, while inverse ROM again represents the lower limit for the composite modulus.

3.5 Thermal properties

Owing to the anticipated application of PPPI-reinforced epoxy composites, the thermal degradation of the material was evaluated *via* thermogravimetric analysis (TGA; see Fig. 12). The incorporation of PPPI clearly leads to an increase in degradation onset temperature (as derived from the onset temperature of the main mass loss). From 313 °C in case of the neat epoxy, the onset is shifted to 364 °C in case of the composite containing 5 vol% PPPI. No significant further increase in degradation onset temperature was found for higher PPPI contents (10 vol% PPPI: 369 °C, 15 vol% PPPI: 370 °C). Note that the onset of thermal degradation of the PPPI filler itself was determined to be 630 °C. Since the enhancement in thermal degradation onset does not increase with filler content beyond 5 vol%, we hypothesize that the effect of the presence of PPPI on thermal degradation is due to a barrier effect of the filler particles resulting in inhibited diffusion of decomposition products into the gas phase, as has been found for similar systems in the literature.[26,43,44]

When comparing the residual mass after heating to 700 °C, the neat epoxy sample exhibits a considerably higher relative residual mass than the composite samples. The neat epoxy sample exhibits a weight loss of 74.7%, while the composite

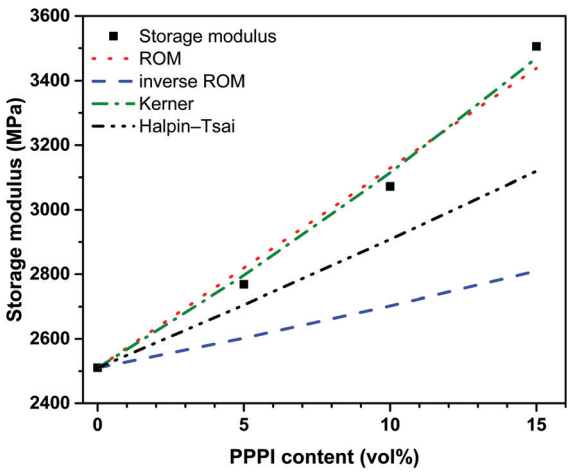

Fig. 11 Storage modulus of PPPI-reinforced epoxy composites as a function of PPPI content comparing the measured values (determined by DMA at 30 °C) and the relationship as predicted by four different estimation models.

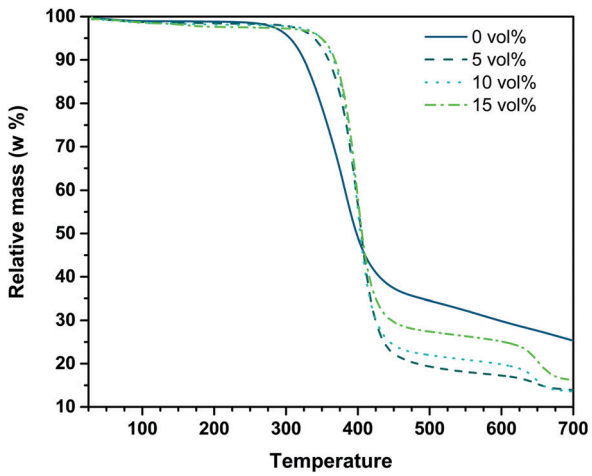

Fig. 12 TGA curves of PPPI-reinforced epoxy for specimens containing different amounts of PPPI filler, measured under nitrogen atmosphere.

samples exhibit weight losses of 83.8% (15 vol% PPPI), 86.4% (10 vol% PPPI), and 86.1% (5 vol% PPPI). The decreased weight loss in the neat epoxy sample is unexpected since the epoxy reference sample should exhibit a lower thermal stability and thus a higher weight loss than the composite samples. This deviation between the neat epoxy and composite samples could either be attributed to changes in the chemical composition of the epoxy matrix (which we expect for the linkage of some of the amine hardener molecules to the epoxy material) or result from kinetic effects introduced by the particle reinforcement, including the provision of escape paths for gaseous decomposition products.

The residual mass of the composite samples before decomposition of the PPPI particles at 630 °C is in accordance to the PPPI content of the composites (24.3%, 19.2%, and 16.8% for 15, 10, and 5 vol% PPPI, respectively).

4. Conclusions

With this work we took a first step towards bringing hydrothermally prepared PPPI of environmentally benign origin and outstandingly high crystallinity closer to real-life applications. In order to achieve this, PPPI microparticles were successfully introduced into an epoxy matrix, resulting in a novel type of PPPI-reinforced epoxy composites.

While the flexural strength of the matrix material was retained with the addition of PPPI up to 15 vol%, the flexural modulus of the composite was increased due to the rigid nature of PPPI. Furthermore, an increase in hardness was observed for the composite materials compared to the base matrix material. Observations from fracture surface analysis indicate a good interfacial adhesion between matrix and reinforcing particles in the composites developed, most likely resulting from an aminolysis reaction occurring between PPPI and the amine hardener compound of the epoxy matrix. The glass transition temperature was found to decrease with increasing PPPI addition, which we attribute to the covalent linking of PPPI to the epoxy matrix consuming a certain fraction of the amine hardener molecules that are therefore not available for crosslinking the epoxy matrix, hence leading to a decrease in the matrix crosslinking density. Yet, the thermal stability of the composite samples was significantly improved.

These results underline that a combination of an amine-based epoxy system and PPPI particles gives rise to a synergistic material behaviour. The use of the high modulus, high strength PPPI particles in the low modulus epoxy matrix leads to a good balance between processing and mechanical properties while at the same time improving the thermal stability, thus rendering these novel composite materials interesting candidates for a wide variety of aerospace, automotive, or sports-equipment-related applications.

Conflicts of interest

There are no conflicts of interest to declare.

Acknowledgements

Funding of this study in the framework of the ''Partnership in Research'' program by the Christian-Doppler-Gesellschaft and the Austrian Science Fund (FWF): PIR 10 is gratefully acknowledged.

References

1 M. A. Meador, Recent advances in the development of processable high-temperature polymers, *Annu. Rev. Mater. Sci.*, 1998, **28**, 599–630.
2 K. Tashiro, Molecular theory of mechanical properties of crystalline polymers, *Prog. Polym. Sci.*, 1993, **18**, 377–435.
3 K. Wakabayashi, T. Uchida, S. Yamazaki and K. Kimura, Micro-flowers of poly (p-phenylene pyromelliteimide) crystals, *Polymer*, 2011, **52**, 837–843.
4 Y. Nagata, Y. Ohnishi and T. Kajiyama, Highly crystalline polyimide particles, *Polym. J.*, 1996, **28**, 980–985.
5 B. Baumgartner, M. J. Bojdys and M. M. Unterlass, Geomimetics for green polymer synthesis: highly ordered polyimides *via* hydrothermal techniques, *Polym. Chem.*, 2014, **5**, 3771–3776.
6 M. J. Taublaender, M. Reiter and M. M. Unterlass, Exerting Additive-Assisted Morphological Control during Hydrothermal Polymerization, *Macromol. Chem. Phys.*, 2018, **219**, 1700397.
7 B. Baumgartner, M. Puchberger and M. M. Unterlass, Towards a general understanding of hydrothermal polymerization of polyimides, *Polym. Chem.*, 2015, **6**, 5773–5781.
8 B. Baumgartner, M. J. Bojdys, P. Skrinjar and M. M. Unterlass, Design Strategies in Hydrothermal Polymerization of Polyimides, *Macromol. Chem. Phys.*, 2016, **217**, 485–500.
9 M. Sajjad, B. Feichtenschlager, S. Pabisch, J. Svehla, T. Koch and S. Seidler, *et al.*, Study of the effect of the concentration, size and surface chemistry of zirconia and silica nanoparticle fillers within an epoxy resin on the bulk properties of the resulting nanocomposites, *Polym. Int.*, 2012, **61**, 274–285.
10 R. Medina, F. Haupert and A. K. Schlarb, Improvement of tensile properties and toughness of an epoxy resin by nanozirconium-dioxide reinforcement, *J. Mater. Sci.*, 2008, **43**, 3245–3252.
11 D. Bazrgari, F. Moztarzadeh, A. Sabbagh-Alvani, M. Rasoulianboroujeni, M. Tahriri and L. Tayebi, Mechanical properties and tribological performance of epoxy/Al_2O_3 nanocomposite, *Ceram. Int.*, 2018, **44**, 1220–1224.
12 A. Bisht, R. M. Kumar, K. Dasgupta and D. Lahiri, Spatial distribution of nanodiamond and its effect on mechanical behaviour of epoxy based composite using 2D modulus mapping, *Mech. Mater.*, 2019, **135**, 114–128.
13 N. Amdouni, H. Sautereau and J. Gerard, Epoxy composites based on glass beads. II. Mechanical properties, *J. Appl. Polym. Sci.*, 1992, **46**, 1723–1735.

14 C. Capela, S. Oliveira and J. Ferreira, Fatigue behavior of short carbon fiber reinforced epoxy composites, *Composites, Part B*, 2019, **164**, 191–197.
15 D. Matykiewicz, M. Barczewski and S. Michałowski, Basalt powder as an eco-friendly filler for epoxy composites: Thermal and thermo-mechanical properties assessment, *Composites, Part B*, 2019, **164**, 272–279.
16 A. Nohales, R. Muñoz-Espí, P. Félix and C. M. Gómez, Sepiolite-reinforced epoxy nanocomposites: Thermal, mechanical, and morphological behavior, *J. Appl. Polym. Sci.*, 2011, **119**, 539–547.
17 O. Zabihi, M. Ahmadi, S. Nikafshar, K. C. Preyeswary and M. Naebe, A technical review on epoxy-clay nanocomposites: Structure, properties, and their applications in fiber reinforced composites, *Composites, Part B*, 2018, **135**, 1–24.
18 S.-Y. Fu, X.-Q. Feng, B. Lauke and Y.-W. Mai, Effects of particle size, particle/matrix interface adhesion and particle loading on mechanical properties of particulate–polymer composites, *Composites, Part B*, 2008, **39**, 933–961.
19 D. Ratna and A. K. Banthia, Rubber toughened epoxy, *Macromol. Res.*, 2004, **12**, 11–21.
20 J. Hodgkin, G. P. Simon and R. J. Varley, Thermoplastic toughening of epoxy resins: a critical review, *Polym. Adv. Technol.*, 1998, **9**, 3–10.
21 M. Sahu and A. M. Raichur, Toughening of high performance tetrafunctional epoxy with poly (allyl amine) grafted graphene oxide, *Composites, Part B*, 2019, **168**, 15–24.
22 D. Paul and C. Bucknall, *Polymer blends: formulations and performance*, New York, Wiley, 2000.
23 R. A. Pearson and A. F. Yee, Toughening mechanisms in thermoplastic-modified epoxies: 1. Modification using poly(phenylene oxide), *Polymer*, 1993, **34**, 3658–3670.
24 J. Cho, J. Hwang, K. Cho, J. An and C. Park, Effects of morphology on toughening of tetrafunctional epoxy resins with poly(ether imide), *Polymer*, 1993, **34**, 4832–4836.
25 C. B. Bucknall and A. H. Gilbert, Toughening tetrafunctional epoxy resins using polyetherimide, *Polymer*, 1989, **30**, 213–217.
26 Y. Chen, L. Sui, H. Fang, C. Ding, Z. Li and S. Jiang, *et al.*, Superior mechanical enhancement of epoxy composites reinforced by polyimide nanofibers *via* a vacuum-assisted hot-pressing, *Compos. Sci. Technol.*, 2019, **174**, 20–26.
27 P. Järvelä and P. Järvelä, Multicomponent compounding of polypropylene, *J. Mater. Sci.*, 1996, **31**, 3853–3860.
28 S. Thomas, K. Joseph, S. K. Malhotra, K. Goda and M. S. Sreekala, *Polymer composites, macro- and microcomposites*, John Wiley & Sons, 2012.
29 Y. Ji, X. Yang, Z. Ji, L. Zhu, N. Ma and D. Chen, *et al.*, DFT-calculated IR spectrum amide I, II, and III band contributions of N-methylacetamide fine components, *ACS Omega*, 2020, **5**, 8572–8578.
30 T. Verdianz, H. Simbürger and R. Liska, Surface modification of imide containing polymers I: Catalytic groups, *Eur. Polym. J.*, 2006, **42**, 638–654.
31 A. Bansal, H. Yang, C. Li, K. Cho, B. C. Benicewicz and S. K. Kumar, *et al.*, Quantitative equivalence between polymer nanocomposites and thin polymer films, *Nat. Mater.*, 2005, **4**, 693–698.
32 R. M. German, *Particulate Composites*, Springer, 2016.
33 S. Ahmed and F. Jones, A review of particulate reinforcement theories for polymer composites, *J. Mater. Sci.*, 1990, **25**, 4933–4942.
34 J. C. Halpin and J. L. Kardos, The Halpin–Tsai equations: A review, *Polym. Eng. Sci.*, 1976, **16**, 344–352.
35 J. Fan and J. Njuguna, An introduction to lightweight composite materials and their use in transport structures, *Lightweight Composite Structures in Transport*, Elsevier, 2016, pp. 3–34.
36 M. Fan, A. Naughton and J. Bregulla, Fire performance of natural fibre composites in construction, *Advanced high strength natural fibre composites in construction*, Elsevier, 2017, pp. 375–404.
37 K. C. Yung, B. Zhu, T. M. Yue and C. Xie, Effect of the filler size and content on the thermomechanical properties of particulate aluminum nitride filled epoxy composites, *J. Appl. Polym. Sci.*, 2010, **116**, 225–236.
38 N. Bleach, S. Nazhat, K. Tanner, M. Kellomäki and P. Törmälä, Effect of filler content on mechanical and dynamic mechanical properties of particulate biphasic calcium phosphate—polylactide composites, *Biomaterials*, 2002, **23**, 1579–1585.
39 S. Goyanes, P. König and J. Marconi, Dynamic mechanical analysis of particulate-filled epoxy resin, *J. Appl. Polym. Sci.*, 2003, **88**, 883–892.
40 O. Becker, R. Varley and G. Simon, Morphology, thermal relaxations and mechanical properties of layered silicate nanocomposites based upon high-functionality epoxy resins, *Polymer*, 2002, **43**, 4365–4373.
41 V. Mathur and K. Sharma, Evaluation of morphological effect on thermal and mechanical performance of PS/PMMA/CdS nanocomposite systems, *Adv. Nanopart.*, 2013, **2**, 205.
42 N. Saba, M. Jawaid, O. Y. Alothman and M. Paridah, A review on dynamic mechanical properties of natural fibre reinforced polymer composites, *Constr. Build. Mater.*, 2016, **106**, 149–159.
43 O. Eksik, S. F. Bartolucci, T. Gupta, H. Fard, T. Borca-Tasciuc and N. Koratkar, A novel approach to enhance the thermal conductivity of epoxy nanocomposites using graphene core–shell additives, *Carbon*, 2016, **101**, 239–244.
44 J. Yu, X. Huang, C. Wu, X. Wu, G. Wang and P. Jiang, Interfacial modification of boron nitride nanoplatelets for epoxy composites with improved thermal properties, *Polymer*, 2012, **53**, 471–480.